Dynamics of Air-Blown Dimples

Renske Gelderloos
Advisors: C.P. Caulfield and A. Belmonte

1 Introduction

A classical problem in fluid mechanics is that of a jet impinging on a solid surface. During the 1960's, partly driven by applications in the steel industry, the exploration of this field of study shifted towards the interaction between a gas jet and a deformable liquid surface (Figure 1), where often the shape of the deformation and its relation to the balance of forces were studied. This is also a very simplified representation of the interaction between the wind and the ocean.

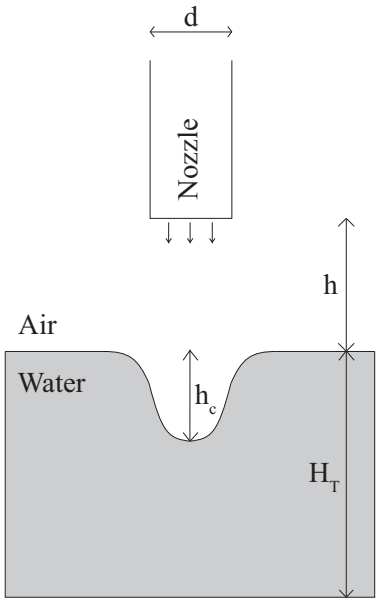

Figure 1: Schematic drawing of the experimental set up. Air is blown from a nozzle at right angles with a still water surface in a tank.

The first report of work on this subject is by Banks and Chandrasekhara (1), who performed experiments with an air jet impinging on a water surface. They identified three regimes: a steady cavity, an oscillating cavity, and splashing. Only the first of these three regimes was studied in more detail and scaling approaches were suggested to establish a relation between the impact of the jet and the depth of the cavity. A few years later Turkdogan (9) performed similar experiments, but included liquids of different densities

in the analysis and especially focused on the relation between the nozzle height and the depth and width of the cavity. Cheslak et al. (3) also studied the geometric properties of a steady air-blown dimple and found simple relations predicting the depth and diameter of the cavities.

A different approach was taken by Olmstead and Raynor (6), who solved the whole shape of steady shallow dimples using conformal mapping. Almost two decades later, new numerical procedures enabled Vanden-Broeck (10) to study slightly deeper cavities with this method, but a conformal mapping approach to this problem without limitations to the depth of the cavity was only provided recently by He and Belmonte (5).

Although instability of the cavity at higher jet-impact velocity was already reported by Banks and Chandrasekhara (1), surprisingly little attention has been given to this phenomenon. The available literature is restricted to predicting the onset of instability, using energy balances to determine the decisive factors. A pioneering study by Rosler and Steward (8) identified two unstable regimes in their experiments: an unstable oscillating regime and a splashing regime. In the former regime three modes of oscillation were identified which were described qualitatively (Figure 2). The onset of the unstable and splashing regimes were shown to depend on a critical jet velocity, with a strong dependence on the interfacial surface tension. Berghmans (2) showed in a theoretical study that increasing liquid density or surface tension is stabilizing, while increasing the gas density is destabilizing. The jet radius was also found to be important.

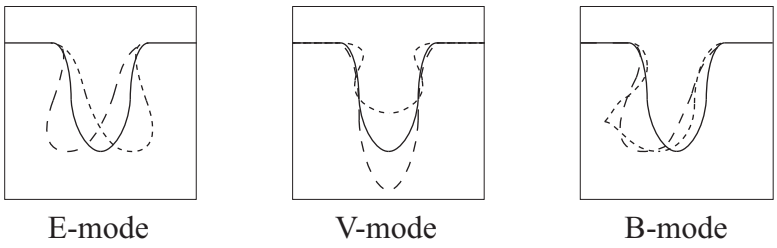

Figure 2: The three modes of instability. In the E-mode the tip of the dimple traces out an ellipse. In the V-mode, the tip oscillates in the vertical direction only. In the B-mode, the tip rolls up the side of the dimple.

The reason behind the sparse coverage of this very interesting problem is likely in the limitations imposed by the available observational equipment. While with the cameras used four decades ago this regime was very difficult to study experimentally, today's high-speed cameras offer the opportunity to capture the movements of the cavity and study them in detail. To our knowledge there is one study (4) in which an attempt was made to study the oscillations of the cavity using a video camera, but no conclusions could be drawn from these results. Here, we use a high speed camera to obtain movies of unstable dimples in a variety of regimes for an air-water system. We explore the dependence of the regimes on key nondimensional parameters and study the spectral properties of the dimple oscillations.

The experimental set up and image processing are discussed in Section 2. The results are first discussed from a qualitative point of view in Section 3. Then a quantitative analysis

is given in Section 4, on the geometric properties of the dimple as well as a spectral analysis of the dimple oscillations. Section 5 discusses the results and gives an overview of the conclusions from this study.

2 Method

2.1 Experimental set up

The jet in the experiment was produced by attaching the wall air supply to a nozzle, which was fixed to an adjustable frame above a layer of water in a tank. The circular nozzle had an inner diameter of 1.35 mm. The square Plexiglas tank was 11.2 cm in height and 20 cm wide. The water depth in the tank was 7 cm unless stated otherwise. To regulate the air flow rate in the jet, a pressure meter (Digital air regulator, Central Pneumatic Professional, model no. 98426) was used. The pressure was calibrated with a volume rate meter (Omega Engineering Gas Mass Flow Meter FMA 1818) to obtain the flow rate Q. The frame to which the nozzle was attached could be moved up and down to adjust its height above the water surface; the position could be read from a calibrated scale. The fluid properties of interest to this experiment are the kinematic viscosity of the gas ($\nu_g = 15.68 \cdot 10^{-6}$ m^2 s^{-1}), the densities of the gas and the liquid ($\rho_g = 1$ kg m^{-3}; $\rho_l = 1000$ kg m^{-3}), and the interfacial surface tension ($\sigma = 71.97$ dyn cm^{-1} $= 71.97 \cdot 10^{-3}$ N m^{-1}). The data acquisition is done with a digital high-speed camera (Phantom v5.0) at a 3000-fps frame rate. Only for the surface views (Section 3.2) the frame rate was adjusted to 300 fps.

2.2 Parameter regime

The two key nondimensional parameters that are varied in this study are the nondimensional nozzle height ($\zeta = h/d$), which determines the distance over which the spreading jet can evolve, and the Reynolds number, which (for fixed ζ) determines the impact pressure of the jet. The Reynolds number is here defined as

$$\mathrm{Re} = \frac{4Q}{\pi\ d\ \nu_g},$$

and varies between $8.5 \cdot 10^2$ and $3.4 \cdot 10^3$. ζ varies between 7.4 and 37.0, equivalent to 1 and 5 cm above the water surface, respectively.

Four other nondimensional parameters, which are mentioned in literature to be important for this problem, are not consciously changed but vary along with ζ and Re. The first is the nondimensional depth of the dimple $\eta = h_c/d$ (variation between 0.8 and 10.0). The second and third are a measure for the importance of surface tension. The Weber number (2; 5), defined as the ratio between inertial forces and surface tension, is given by

$$\mathrm{We} = \frac{\rho_g \left(\frac{Q}{1/4\pi d^2}\right)^2 r_{\mathrm{jet}}}{\sigma},$$

and varies in our experiments between 1.4 and 105 The Bond number (2; 5), which is the ratio between gravitational forces and surface tension, is given by

$$\mathrm{Bo} = \frac{(\rho_l - \rho_g)\ \ g\ r_{\mathrm{jet}}^2}{\sigma},$$

and varies between 0.1 and 3. The last nondimensional number of importance to this study is the Froude number (1), which is defined as the ratio between a characteristic velocity and a gravitational wave velocity:

$$\mathrm{Fr} = \frac{\left(\frac{Q}{1/4\pi d^2}\right)}{\sqrt{g h_c}},$$

and varies between 107 and 127 in our experiments. The dynamics of the surface waves were however not studied here quantitatively.

2.3 Image processing

A five-step process was followed in obtaining the contours of the cavity from the movies (Figure 3). First the black and white avi movies, captured with the high-speed camera, were loaded into Matlab and separated into individual frames (Figure 3a). Second, to maximize the amount of information that could be extracted from the movie frame, the contrast in the images was enhanced using CLAHE (Contrast-Limited Adaptive Histogram Equalization, Figure 3b). This technique determines the histogram of the grayscale values of the pixels for small regions in the image and then enhances the contrast in such a way that the histogram of the output approximately matches a uniform distribution. Neighbouring tiles are combined using bilinear interpolation to eliminate artificially induced boundaries. An edge detection scheme is applied on the filtered image to define the shape of the cavity (Figure 3c). Note that the contrast enhancement step improves the result of the edge detection considerably, especially tracing the shallow part of the cavity (Figure 4). The Sobel method was found to give the best representation of the deep as well as the shallow part of the cavity shape. This method calculates the first derivative of the grayscale intensity in both x and y directions, and locates the edge at minimum and maximum values of this gradient as long as this value exceeds a certain threshold value. Last, the outer contour of the cavity was traced by moving upward along the vertical direction in the frame and tracing the first 'edge-point' for every column (Figure 3d). The shapes thus obtained were lowpass filtered to reduce artificial noise introduced in the detection process, before statistics such as the cavity depth, the angle with the vertical, and frequencies were calculated. These are discussed in Section 4. For the spectral analysis the time series were first detrended, after which a Hann filter was applied. The frequency spectrum was calculated using a FFT algorithm.

3 Experimental phenomenology

3.1 Cavity

A variety of shapes and movements of the dimple are observed in the experiments. In Figure 5 the sequence of modes is shown when the Reynolds number of the jet is increased while the nozzle height is fixed at the lowest position considered in this study ($\zeta = 7.4$). For low jet Reynolds numbers the cavity is stable and slowly deepens when the jet flow is increased (Figure 5a). We will refer to this state as the S-mode. At a critical value of $\mathrm{Re} = 1075$ instability sets in and the tip of the dimple traces out an ellipse (E-mode, Figure 5b). This mode only exists for a very narrow range of the jet Reynolds number, as it quickly changes

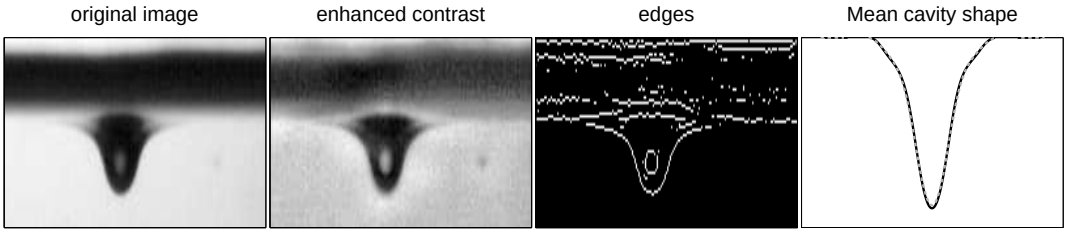

(a) (b) (c) (d)

Figure 3: From the original image frame to a cavity outline. First the contrast is enhanced using CLAHE (b), then the edge is detected using the Sobel method (c). The contour of the cavity is found from the detected edges (black solid line in (d)), and lowpass filtered for further analysis (gray dotted line in (d)). ($\zeta = 7.4$, Re = 1050)

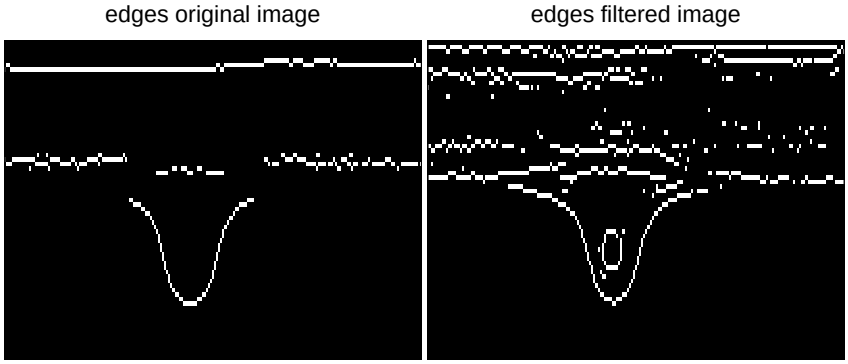

(a) (b)

Figure 4: Improvement in the edge detection results due to contrast enhancement.

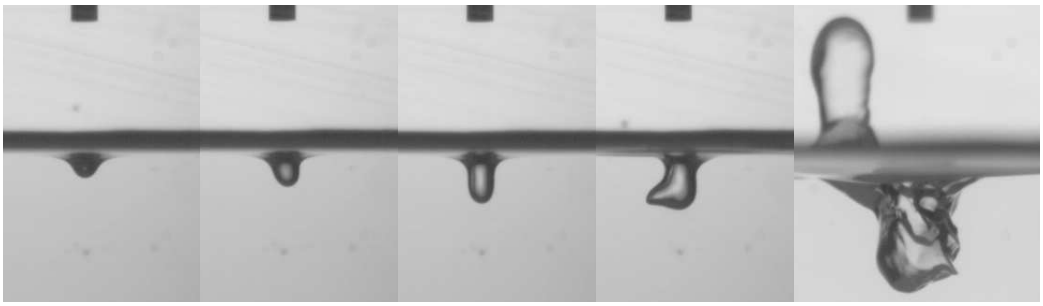

(a) S-mode (b) E-mode (c) V-mode (d) B-mode (e) Bubbling and splashing

Figure 5: Subsequent stages of the dimple with increasing jet Reynolds number for a fixed nozzle height ($\zeta = 7.4$). (a) A stable dimple (Re = 1030). (b) The tip traces out an ellipse (Re = 1075). (c) The tip moves up and down vertically (Re = 1095). (d) The tip bends and rolls up the side of the dimple (Re = 1230). (d) Bubbling and splashing (Re = 3360).

into a purely vertical oscillation of the tip, here referred to as the V-mode (Figure 5c). If the flow rate in the jet is increased even further, the tip starts to bend and roll up the side of the dimple, which we call the B-mode (Figure 5d). At very high Reynolds numbers (Figure 5e) bubbling and splashing is observed.

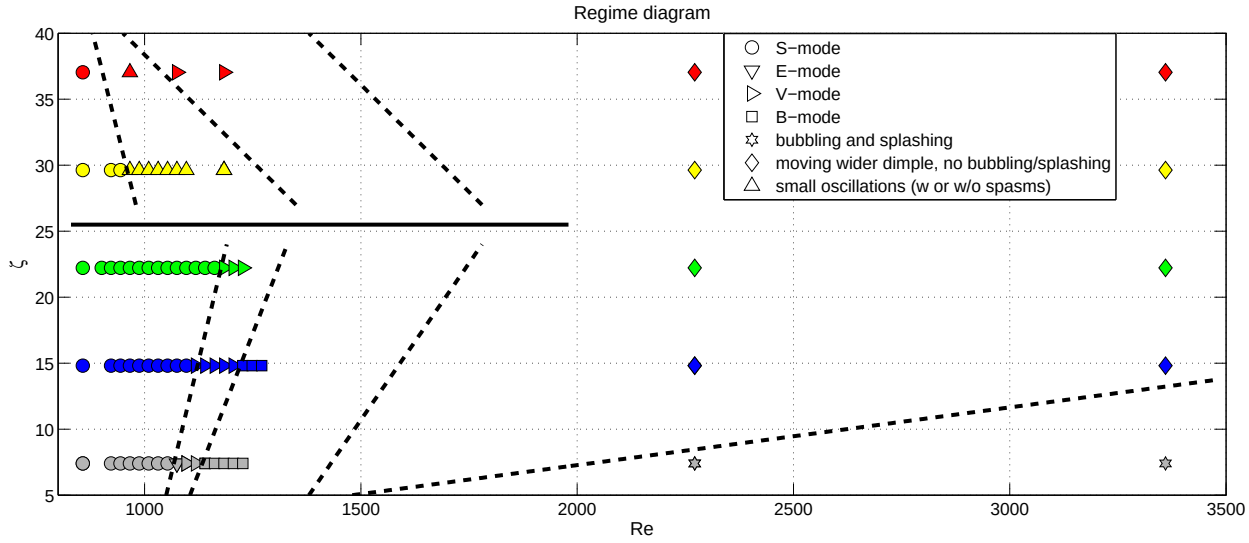

Figure 6: Overview of the observed regimes as a function of the jet Reynolds number Re and the nondimensional nozzle height ζ.

The onset of the next mode shifts to different Reynolds numbers at the other nozzle heights considered in this study. The regime diagram in Figure 6 shows the observed modes for several combinations of ζ and Re. A first interesting feature from this graph is the increase in Reynolds number required for instability with ζ for the lowest three values of ζ considered (beneath the solid black line in Figure 6). For the larger nozzle heights, the required Reynolds number decreases with ζ. Although the measurements are sparser in the remainder of the regime diagram, this seems to be a robust feature as indicated by the speculative dashed lines. Also, in the two largest ζ cases the dimple starts 'shivering' when it is still stable, i.e. there are very small, noise-like oscillations. It is well known that it takes a distance of about 30 nozzle diameters for a turbulent jet to become fully developed (7). We therefore believe that the horizontal solid line indicates the nozzle height above which the jet shows fully developed turbulence. The noise-like behaviour above this height is then due to instability of the jet rather than an instability of the dimple.

A second result from this figure is that for all the nozzle heights except for the smallest one, the dimple widens at high Reynolds number (Figure 7b, a stable small dimple is given in Figure 7a for comparison). We speculate that the width of the dimple is in general restricted by the interfacial surface tension, but that the high impact pressure of the higher Reynolds number jet is able to overcome the surface tension and creates a wider dimple. At very small ζ the dimple displays bubbling and splashing behaviour. It is expected however that the dimple will enter the splashing state at the larger nozzle heights as well at even higher jet Reynolds numbers, which were not currently studied. It should be noted that the

modes are not entirely identical for the different nozzle heights. For example, at $\zeta = 24.4$ the V-mode is a very elegant one and resembles a Mexican hat (Figure 7c). However, the overall behaviour is the same.

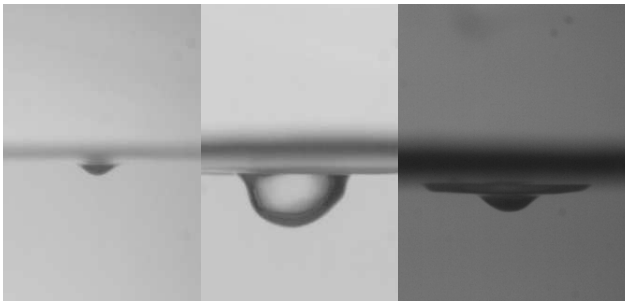

(a) (b) (c)

Figure 7: Snapshots (a) Stable dimple: $\zeta = 22.2$, Re = 990 (b) Wide oscillating dimple: $\zeta = 14.8$, Re = 2270 (c) The "mexican hat", a very elegant V-mode: $\zeta = 24.4$, Re = 1400

In this study we focused on an air-water system. The influence of interfacial surface tension σ and liquid viscosity ν_l were studied briefly as well from a qualitative point of view only. The surface tension was altered by adding 2-3 drops of dish-washing liquid (Ajax Lemon) to the water in the tank, which decreased the stability of the dimple. To test the influence of viscosity, the tap water was replaced by glycerol and water-glycerol mixtures. The experiments clearly showed increased stability of the dimple, but were not conclusive quantitatively.

3.2 Surface

While motions of the liquid phase are consistently neglected in analyses presented in literature, the observed motion shows an interesting pattern. When the cavity is in the S-mode and thus not moving, the flow at the surface displays a saddle-point like pattern at the location of the dimple, with water flowing in from two sides and flowing out in the perpendicular directions. It starts up as soon as the jet is switched on, and ceases when the air source is switched off. When the air rate is turned up, waves are formed at the surface which spiral out from the cavity (Figure 8a) accompanying the E-mode. At higher Reynolds number the surface waves were more axisymmetric (Figure 8b) and increased in amplitude with increasing jet Reynolds number. The wave formation was clearly triggered by the dimple oscillations, but a quantitative analysis of the surface phenomena are beyond the scope of this study.

4 Data analysis

4.1 Geometric properties of the dimple

The cavity depth (h_c in Figure 1) increases with increasing jet strength and decreases with increasing nozzle height. This is shown in Figure 9a, where the symbols correspond to the

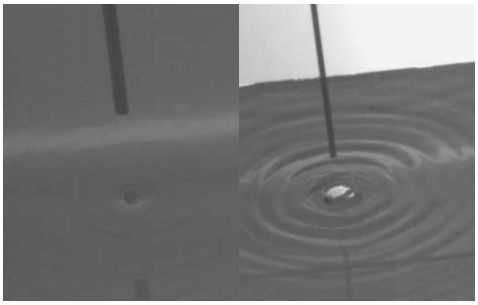

(a) (b)

Figure 8: Snapshots of the surface wave field (a) E-mode: $\zeta = 7.4$, Re $= 1075$ (b) Bubbling and splashing: $\zeta = 14.8$, Re $= 2270$

cavity depth, averaged over all frames of a single movie with the corresponding jet strength Re (x-axis) and nozzle height ζ. The colour coding for ζ and symbols for mode of instability are the same as used in Figure 6. The low-Reynolds number regime is enlarged in Figure 9b. The maximum cavity depth, which is a more objective measure for oscillating dimples, is plotted in Figures 10a and 10b. (Note that cavity depths on the red line ($\zeta = 37.0$) exceed the values on the yellow line ($\zeta = 29.6$) in the low-Reynolds number regime. This is not a physical feature however, but a result of increasing difficulty in obtaining sharp images as the bottom of the cavity approached the meniscus.) The area of the two-dimensional image of the cavity shows a similar behaviour (not shown).

The depth of the stable cavities slowly increases when the jet strength is raised (generally Re < 1050). Then a clear difference is observed between the three smallest nozzle heights and the two larger ones. In the former case, the cavity depth raises quickly between a Reynolds number of approximately 1050 and 1200, around the point of instability. In the latter case the cavity depth only increases slightly over this range of Reynolds numbers. This is in line with the preliminary conclusion from Figure 6 in Section 3.1 that the behaviour of the dimple is different for the larger two nozzle heights: the turbulence in the jet is already fully developed and therefore the peak velocity is lower at impact. The jet is therefore unable to exert a large enough pressure on the water surface to deepen the dimple further.

A second interesting property is the evolution of the curvature of the cavity as the jet strength is increased. In Figure 11 the maximum curvature is given for the lowest three nozzle heights (the jet does not form a stable cavity over a range of Re at larger nozzle heights and the curvature can therefore not be determined well). As the point of instability is approached, the maximum curvature quickly increases. The lines suggest that instability sets in when a critical value of the curvature is exceeded, around $11 \cdot 10^{-3}$. Figure 10a suggests that a similar critical value of the cavity depth (or jet impact velocity) may exist for the onset of the bubbling and splashing phase. In the current set of experiments this critical depth, which is at 11 to 12 mm, is only reached in the smallest ζ case.

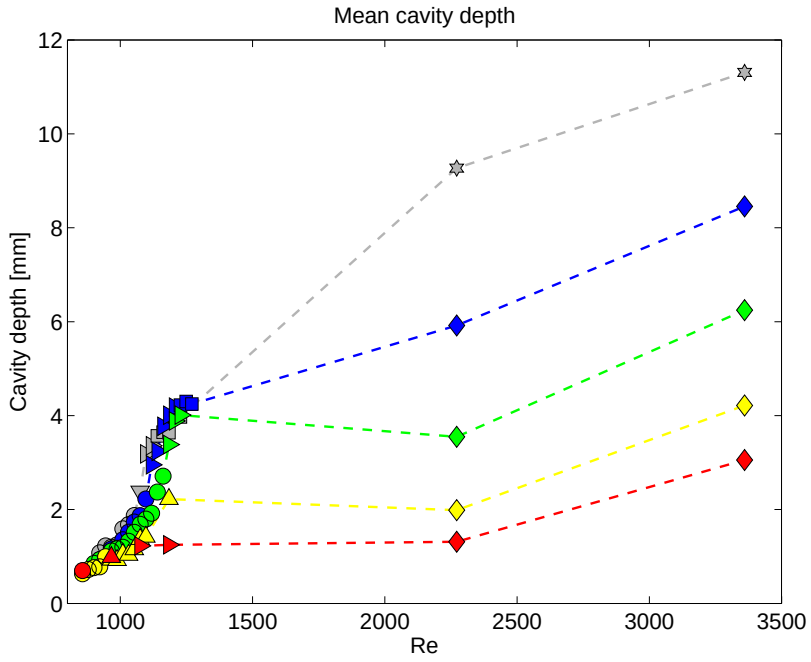

(a)

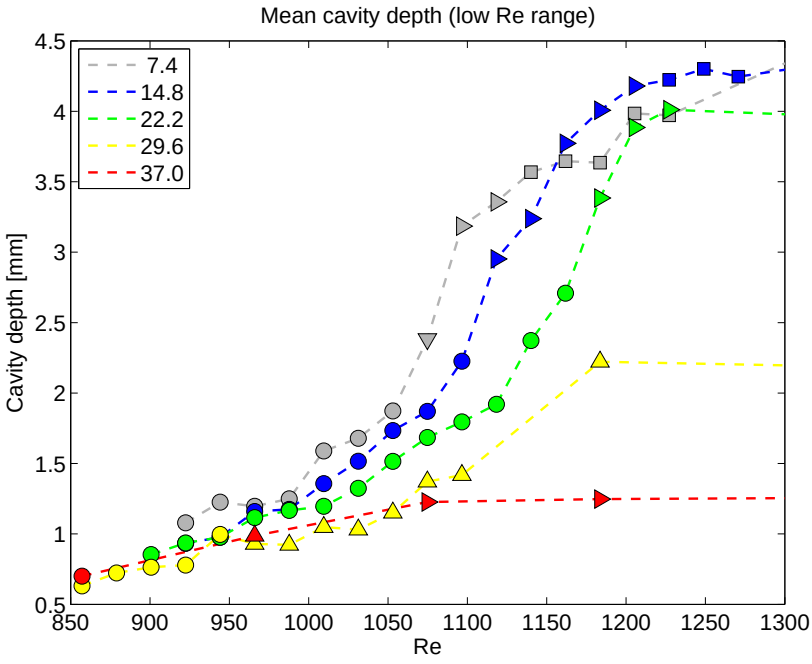

(b)

Figure 9: Mean cavity depth h_c as a function of the jet Reynolds number. The colours and symbols are as in Figure 6.

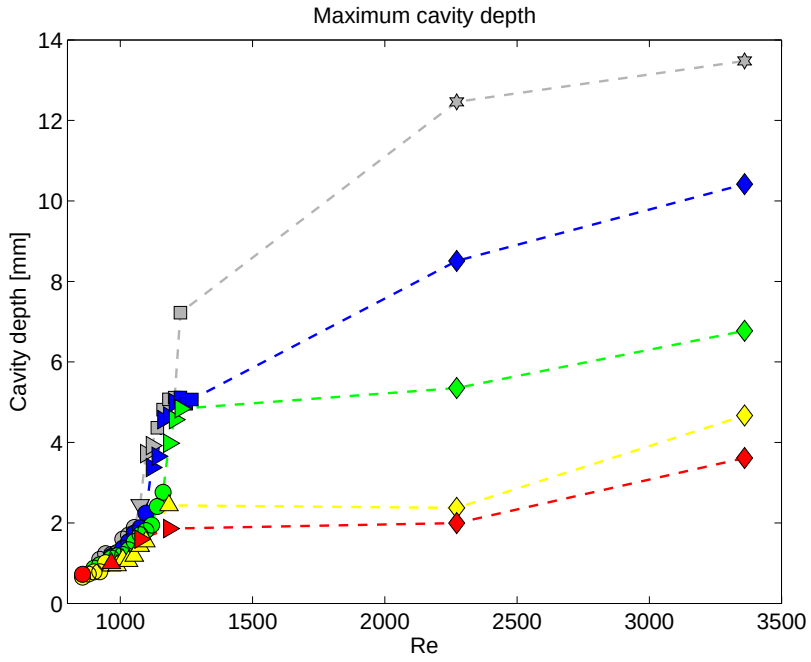

(a)

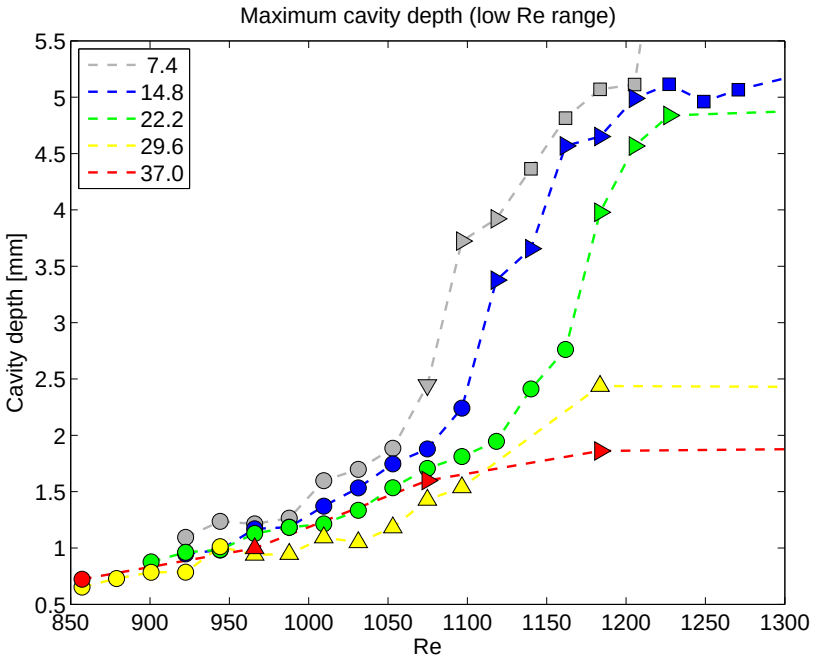

(b)

Figure 10: Maximum cavity depth h_c as a function of the jet Reynolds number. The colours and symbols are as in Figure 6.

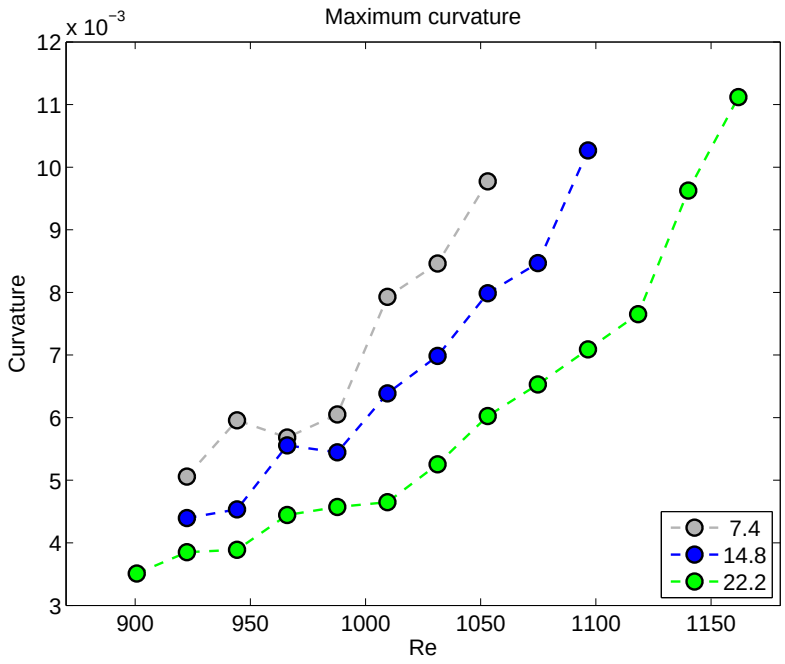

Figure 11: Maximum curvature of the cavity outline as a function of the jet Reynolds number for the stable cavities. The colours and symbols are as in Figure 6.

4.2 Dimple dynamics

The geometric properties of the dimple were described above. In this section the behaviour of the dimple in time is analyzed. A first impression of the differences between different modes of oscillation is presented in Figure 12. The cavity depth and angle with respect to the vertical [1] are drawn for the E-mode (left panels), the V-mode (middle panels), and the B-mode (right panels) at nozzle height $\zeta = 7.4$. The E-mode only shows very slight oscillations in depth, but very regular oscillations in the angle time series. The angle in the V-mode on the other hand is, as expected, almost zero, with clear oscillations in the depth series. The B-mode shows oscillations in both depth and angle. As the behaviour of the dimple in the B-mode seemed fairly chaotic at first sight, the oscillations are remarkably regular. In contrast to the E-mode, with one clear frequency, and the V-mode, which has a more intermittent behaviour, the signal shows multiple frequencies with a clear periodicity.

The frequency spectra of the three modes of instability (Figure 13) show spectral peaks at slightly different frequencies. The E-mode has a peak around 55 Hz in the power spectra of cavity depth and angle with the vertical. A second peak is found in the depth spectrum at twice the 55 Hz frequency, around 108 Hz, that is larger than the 55 Hz peak. This higher frequency mirrors the double crossing of the vertical in the apparent pendulum-like movement of the dimple in the 2-dimensional image of the 3-dimensional elliptical

[1] This angle is defined as the angle between the axis of symmetry (the continuation of the centerline of the jet) and the line drawn from the crossing of the centerline of the jet and the water surface to the tip of the dimple.

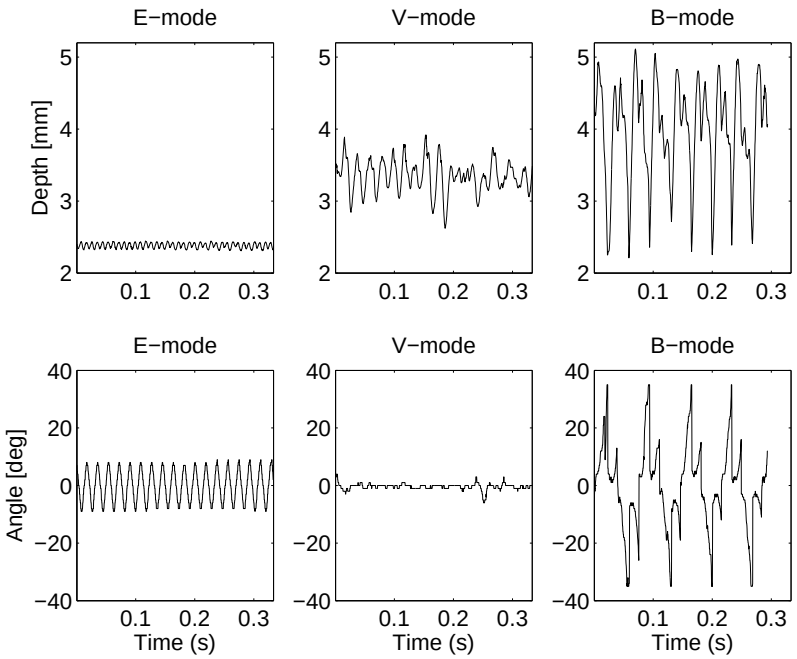

Figure 12: Cavity depth (upper panels) and angle of the cavity with the vertical (lower panels) from time series in the E-mode (left panels), the V-mode (middle panels), and the B-mode (right panels) at nozzle height $\zeta = 7.4$.

movement. The V-mode spectrum is more noisy, but shows the highest peak around 52 Hz in the depth series, comparable to the E-mode. As expected, no distinct peaks are observed in the angle power spectrum. Last, the spectra of the B-mode time series show a high peak at low frequency (14.5 Hz in the angle spectrum and twice this value, 29 Hz, in the depth spectrum) with lower peaks at higher harmonics. One of the peaks is at 57 Hz, again comparable to the 55-Hz peak in the E-mode spectra. Although the exact values of the frequency peaks slightly differ, we not believe them to be actually different and the fundamental oscillation frequency does therefore not seem to change as the dimple oscillation enters another mode.

Figure 14 shows the frequency spectra for the highest Reynolds number considered at the different nozzle heights. Unlike the spectra at one nozzle height, the spectral peak shows up at increasingly lower frequency for increasing nozzle height. (An exception is in the $\zeta = 29.6$ line, which does not show one clear peak at all because the jet is going turbulent around this nozzle height.) The same behaviour, but less distinct, is observed at the other high-Reynolds number measurements. For the lower Reynolds number regime, no such pattern is found.

In the regime diagram (Figure 6) a separate mode was assigned to the seemingly stable cavities at higher nozzle heights which showed very small and rapid oscillations. This shivering-like behaviour does not seem to be an oscillation of the dimple itself. An example of a time series in this mode is give in Figure 15. The larger troughs were probably dust particles or other disturbances swept through the cavity by the surface flow. The smaller

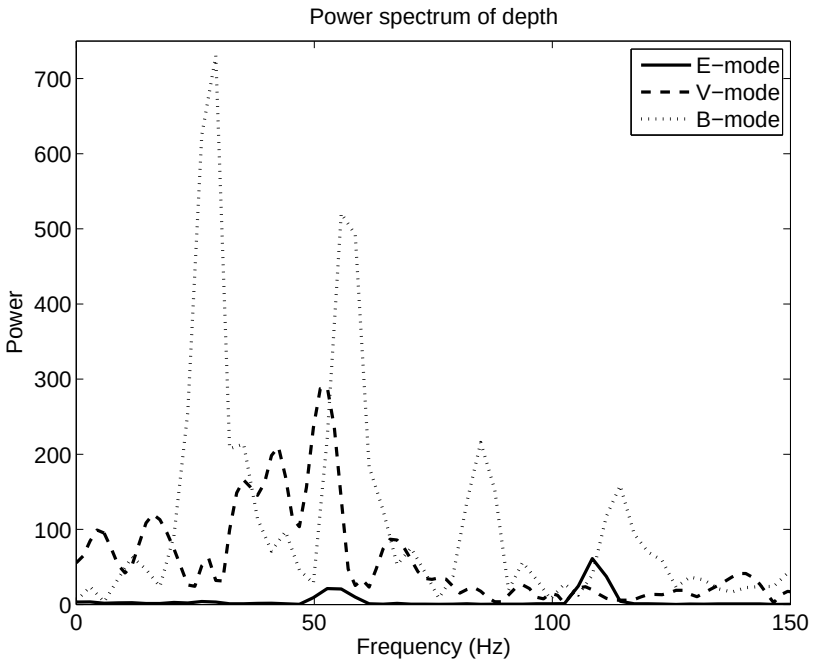

(a)

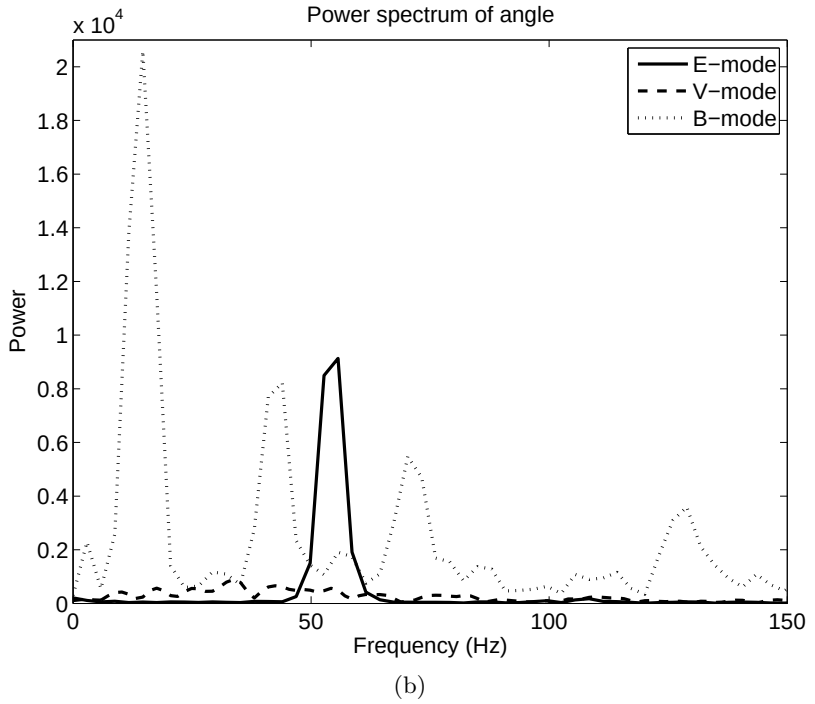

(b)

Figure 13: Power spectra of the time series from Figure 12.

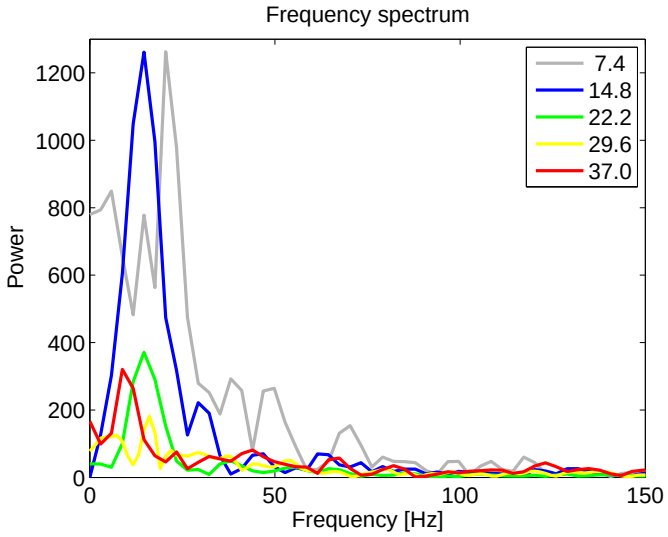

Figure 14: Frequency spectra of the time series at Re = 3360. The line colours for nozzle heights are as in Figure 6.

noisy oscillations are the observed small and rapid oscillations. The frequency spectrum of the middle part of the time series confirms that there is no clear spectral peak at high frequency. These oscillations are thus indeed noise. The noise is likely caused by the increased turbulence in the jet, which has more time to develop at the larger nozzle height.

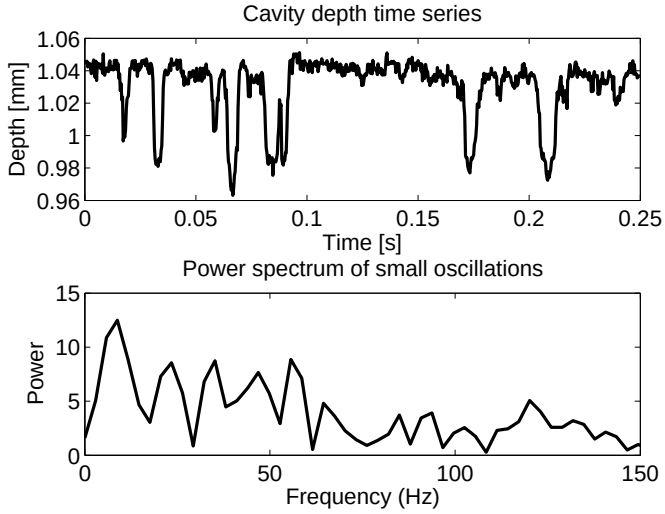

Figure 15: Time series of the cavity depth and its frequency spectrum at $\zeta = 29.6$ and Re = 1030.

5 Discussion and Conclusions

The behaviour of a dimple that is formed by an air jet impinging at right angles on a water surface was studied. In particular the dependence of the geometric properties, onset of oscillation and modes of oscillation were studied as a function of the air flow rate at the nozzle, defined as the jet Reynolds number, and the source height, given by the nondimensional nozzle height.

At low jet Reynolds number a stable cavity is formed. When the air flow rate is turned up, a sequence of oscillation modes is observed. The range over which the modes of oscillations are found depends on the nozzle height. Also not all unstable modes are observed at every nozzle height considered. The unstable modes identified were:

- E-mode: The tip of dimple traces out an ellipse. This mode was only found at the smallest nozzle height and shows very regular oscillations.
- V-mode: The dimple oscillates vertically. This mode was found at all nozzle heights except for the fourth one. The regime diagram however indicates that the Re-range where this mode is expected at the fourth nozzle height is not sampled in this study. The oscillations in this mode are sometimes rather regular, but other times they showed more intermittent behaviour (see e.g. the upper middle panel in Figure 12).
- B-mode: The oscillation overshoots, and the tip of the dimple bends and rolls up the side of the dimple. This mode was observed at the lowest two nozzle heights. Again, the Re-range at which this mode is expected at the higher nozzle heights was not sampled. The oscillations in this mode are again very regular.
- At the largest nozzle heights, very small oscillations of the dimple are observed at low jet Reynolds number, which shows up as noise in the time series. We speculate this is due to an instability of the jet.
- In the high Reynolds number range two other modes are found:
  - Bubbling and splashing. This mode is only observed at the lowest nozzle height, but will probably eventually set in at higher nozzle heights as well if the flow rate is increased further. It seems that a critical dimple depth exists above which this mode sets in.
  - A widening of the dimple. We believe this shape to arise when the jet overcomes the surface tension. This mode is not observed at the lowest nozzle height.

Two distinctively different regimes are found. For the smallest three nozzle heights, the Reynolds number at which a next mode of oscillation is entered increases with increasing nozzle height. For the largest two nozzle heights on the other hand the required Reynolds number for a certain mode of oscillation decreases with increasing nozzle height. Also, the cavity depth increases rapidly around the point of instability for the smallest three nozzle heights, while it only increases slightly in the larger two cases. Overall, the depth of the cavity increased with increasing jet strength and decreases with increasing nozzle height. The difference in cavity depth with nozzle height is small at low jet Reynolds number and larger at high jet Reynolds number.

Clear evidence is found for two competing effects in the system as the air flow rate in the jet is increased. If both the nozzle height and the flow rate are small, the dimple depth increases with increasing flow rate until the dimple becomes unstable. If the nozzle is sufficiently far away from the water surface however, turbulence develops in the jet when the flow rate is high enough. In a turbulent jet the velocity decreases with distance from the nozzle and the rate of increase of impact of the jet therefore levels off.

The time dependent behaviour of the dimple oscillations was studied using their frequency spectra. The spectra suggest that the frequency does not change much when the nozzle height is fixed (spectral peaks at different higher harmonics do show up with increasing Reynolds number). For the smallest nozzle height a fundamental frequency around 55 Hz is found. This frequency can be linked to the waves produced on the surface. The dispersion relation for deep water gravity waves is $\omega = \sqrt{gk}$. With $\omega = ck$, $c = \lambda/T$, and $k = 2\pi/\lambda$, the frequency of the wave is found from

$$\frac{1}{T} = \sqrt{\frac{g}{2\pi\lambda}},$$

where ω is the angular frequency, c the phase velocity, k the wave number, T the wave period, and λ the wave length. If the dimple represents half a wave, the wave length is twice the dimple width. The small dimples are about 1 mm wide, giving a frequency of 28 Hz. The fundamental frequency of 55 Hz is twice this frequency. At the higher Reynolds numbers the largest peak in the spectrum shifts to a lower frequency with increasing nozzle height. It should be noted that not all spectra show clear narrow peaks. As the filter removes part of the time series, perhaps longer time series would give a better result. Also ensemble measurements with more than one time series per $\mathrm{Re} - \zeta$ pair could increase the signal-to-noise ratio, especially in the modes where the dimple oscillations are irregular.

A few open question remain after this study. In particular, it would be very helpful to know more about the air jet itself. Visualization of the jet would provide information on the formation of turbulence, the radius at impact and its relation to the dimple radius. Without specific information on the jet, it is very difficult to form an idea of the physics involved, and results remain speculative.

Secondly, surface tension seem to be an important factor in the dimple stability. This was already confirmed by earlier studies (in particular Rosler and Steward (8)). If the radius of the jet could however be measured accurately in this study, the Bond and Weber number can be calculated and related to the jet Reynolds number and the nozzle height (the jet spreads and thus reaches a larger radius at impact at larger nozzle height). This is likely to shed a more physical light on the now speculative lines in the regime diagram.

Thirdly, measurements should be added in the regime diagram in the 700 to 1500 Reynolds number range, in particular where the speculative lines suggest the presence of a certain mode at a certain nozzle height which is not yet confirmed due lack of data.

References

[1] R. Banks and D. Chandrasekhara, *Experimental investigation of the penetration of a high-velocity gas jet through a liquid surface*, Journal of Fluid Mechanics, 15 (1963), pp. 13–34.

[2] J. Berghmans, *Theoretical investigation of the interfacial stability of inviscid fluids in motion, considering surface tension*, Journal of Fluid Mechanics, 54 (1972), pp. 129–141.

[3] F. Cheslak, J. Nicholls, and M. Sichel, *Cavities formed on liquid surfaces by impinging gaseous jets*, Journal of Fluid Mechanics, 36 (1969), pp. 55–63.

[4] M. Evestedt and A. Medvedev, *Gas jet impinging on liquid surface: cavity shape modelling and video-based estimation*, (2005).

[5] A. He and A. Belmonte, *Deformation of a liquid surface fue to an impinging gas jet: A conformal mapping approach*, Physics of Fluids, 22 (2010), pp. 042103–1 – 042103–7.

[6] W. Olmstead and S. Raynor, *Depression of an infinite liquid surface by an incompressible gas jet*, Journal of Fluid Mechanics, 19 (1964), pp. 561–576.

[7] S. Pope, *Turbulent flows*, Cambridge University Press, Cambridge, 2000.

[8] R. Rosler and G. Stewart, *Impingement of gas jets on liquid surfaces*, Journal of Fluid Mechanics, 15 (1968), pp. 13–34.

[9] E. Turkdogan, *Fluid dynamics of gas jets impinging on surface of liquids*, Chemical Engineering Science, 21 (1966), pp. 1133–1144.

[10] J. Vanden-Broeck, *Deformation of a liquid surface by an impinging gas jet*, SIAM Journal of Applied Mathematics, 41 (1981), pp. 306–309.